J Mater Sci (2023) 58:880–889

A 3D pillar hydrogel assembled from multi-metallic oxides nanoparticles for plasmon-enhanced solar interfacial evaporation

Huihua Min[1], Deqi Fan[2], Hao Zhang[1], Xueling Xu[1], Xiaofei Yang[1], and Yi Lu[1,*]

[1] College of Science, Advanced Analysis and Testing Center, Nanjing Forestry University, Nanjing 210037, People's Republic of China
[2] College of Chemical Engineering, Nanjing Forestry University, Nanjing 210037, People's Republic of China

Received: 13 August 2022
Accepted: 30 November 2022
Published online:
16 December 2022

ABSTRACT

Harvesting solar energy to convert thermal energy is a promising technology that enables substantial eco-friendly applications to alleviate freshwater and energy crisis. To realize rapid and energy-efficient solar driven steam evaporation, developing efficient photothermal conversion materials are significantly important. Here is a facile approach for constructing a three-dimensional (3D) pillar hydrogel based on $FeCoNiCrO_x$ (FCNCO) for effective water treatment. Taking advantage of high solar absorption property and low evaporation enthalpy, the CPH-2S can be capable of achieving surface plasmon resonance assisted water evaporation rates of 2.44 kg m^{-2} h^{-1} under 1 sun irradiation. This function endows the evaporator with a light-to-vapor conversion efficiency of 96%, which is induced by an elaborately constructed hydrogel with surface photons trapping and thermal localization capabilities. Meanwhile, the hydrogel exhibits salt resistance in seawater as well as the stability of solar evaporation performance. This work offers a rational design principle to create multi-metal component-based photothermal materials for developing a self-sustainable and solar-powered water-energy platform.

Introduction

With the fast-growing population, the demand of freshwater resources has increased over the past few decades. Developing sustainable technologies to supply, a large amount of freshwater is becoming much more pressing [1, 2]. Amongst these technologies, seawater desalination technology has been regarded as one of the most promising strategies to produce freshwater by exploiting seawater resources, which accounts for 97% of water resources on the earth. Effective utilization of solar energy is one of the most promising pathways to produce

Handling Editor: Kevin Jones.

Address correspondence to E-mail: yilu@njfu.edu.cn

https://doi.org/10.1007/s10853-022-08055-1

green energy resources [3–5]. Nowadays, an emerging solar driven interfacial desalination technology provides a cost-effective and sustainable pathway to continuously produce clean water, compared to the membrane distillation technology of high cost and energy consumption [6–8]. Specifically, solar energy harvested by photothermal materials convert into thermal energy to vaporize the liquid water for purification purposes. Benefiting from the advantages of inexhaustible solar energy and zero carbon emission process, the solar driven interfacial evaporation that utilize solar energy to localize heat for water evaporation is a great potential candidate to tackle water and energy scarcity [9]. Hence, an efficient solar-powered photothermal material that can perform the full solar spectrum is highly anticipated.

Over the past decades, solar interfacial evaporation systems mainly focus on the selection of photothermal materials as well as elaborate design of evaporation structures [10–13]. Many efforts have been devoted to employing metallic materials, carbon-based materials or polymer as photothermal materials [14, 15]. As a member of metallic based materials, the multi-transition metal oxides (M-TMOs) are attracting increased interests due to their unique advantages in broadband light absorption, good thermal stability, and fabrication feasibility [16–18]. However, there are few investigations about applying M-TMOs as solar receivers, which possess unique optical properties and widely used in photocatalysts, solar cells, photothermal conversions, photoelectrochemical conversions, etc. Recently, high-entropy alloy FeCoNiTiVCrCu nanoparticles was developed by Zhang's group, in which the *d-d* interband transitions of 3d electrons in transition metals lead to strong solar absorption for efficient photothermal conversion [19]. Liu et al. reported a solid-solution alloy with multi-principal elements (AlCrWTaNbTiN) as an effective absorption layer to obtain a high solar absorptance of 93% [20]. Abraham utilized transition metals (Mn, Ni and Cu) to dope Sb_2O_3 to modify the optical property [21]. Moreover, the localized surface plasmon resonance (LSPR) effect of transition metal oxides was employed for the photothermal conversion in the applications of solar steam generation [22, 23]. Thus, it's significant to further explore M-TMOs as absorbers with the widen absorption spectra and stimulate the scope of their utilization in the fields of high-performance water evaporation.

To construct a satisfactory solar evaporator, the functional M-TMOs can be incorporated into hydrogels to form hydrogel-based evaporators, as the microchannels in the hydrogel can facilitate water transport and gas escape. The hydrophilic polymeric networks can confine the solar heat and continuously replenish water to the top surface. Moreover, the distinct polymeric composites can activate water molecules and reduce the energy requirement for water vaporization. Herein, we designed a 3D pillar hydrogel containing multi-transition metal oxides with effective photothermal conversion to achieve rapid solar steam generation. The premise for our design is that the FCNCO acts as plasmonic waveguide for the rapid conversion of solar photons into confined thermal energy. Moreover, the hydrogel features a hydrophilic interconnected porous structure for water transport and vapor escape. Benefited from the light trapping of surface pillar structure, the optimized evaporator can achieve efficient solar evaporation, offering a beneficial inspiration and reference for high-performance photothermal materials in solar steam generation applications.

Experimental methods

Preparation of metal oxides, hydrogels and 3D pillar solar evaporator

Materials

$Fe(NO_3)_3\cdot 6H_2O$, $Co(NO_3)_2\cdot 6H_2O$, $Ni(NO_3)_2\cdot 6H_2O$, $CrCl_3\cdot 6H_2O$, citric acid, absolute ethyl alcohol, polyvinyl alcohol (PVA), cellulose (CS), ammonium hydroxide, glutaraldehyde and hydrochloric acid are purchased from Aladdin. The chemicals are used without any further treatment.

Synthesis of FeCoNiCrO$_x$ oxides

$Fe(NO_3)_3\cdot 6H_2O$ (0.808 g), $Co(NO_3)_2\cdot 6H_2O$ (0.582 g), $Ni(NO_3)_2\cdot 6H_2O$ (0.594 g) and $CrCl_3\cdot 6H_2O$ (0.544 g) were dissolved into the mixture solution of water (75 mL) and ethanol (15 mL) with constant stirring. A certain of ammonium hydroxide and citric acid (0.362 g) was added to the above solution until the pH of the solution was 7. After that, the mixture was heated by water bath at 90 °C to obtain a gel. The solid gel was then maintained at 240 °C for 3 h in a furnace and consequently calcinated at 1000 °C for 3 h under an Ar/N_2 atmosphere.

Synthesis of transition metal oxides solution-based hydrogels

Firstly, PVA (4 g, 5 wt% in water) and cellulose solution (1 g, 0.6 mmol/g) were mixed at 60 °C in breakers. Subsequently, the PVA/CS hydrogel was prepared by adding hydrochloric acid (225 μl, 1 mol/L) and glutaraldehyde (200 μl, 5 wt%). Then, the gel was poured into specific moulds, subsequently by freezing and thawing for several times. Finally, the formed hydrogel was circularly immersed into water and ethyl alcohol to remove the impurities, which was labeled as CPH-0. The details of preparation process for the other hydrogels in this work were similar to that in our previous works [24, 25], except that the addition of the $FeCoNiCrO_x$. The samples were labeled as CPH-1, CPH-2, CPH-3, according to the amount of the $FeCoNiCrO_x$ (20, 30, 40 mg). To further architect the surface structure, we employed the pillar array mould to form the CPH-2S.

Materials characterization

The X-ray diffraction (XRD, Ultima IV, Rigaku) spectrum and Fourier transform infrared spectroscopy (FTIR, VERTEX 80 V, Bruker, Germany) were performed to measure and analyze the phase of the composites. The Rietveld refinements of the X-ray diffraction patterns were performed using GSAS software. The microstructure of the samples was observed using scanning electron microscopy (SEM, JSM-7600F, Japan). The water-droplet contact angle was tested using a contact angle instrument (KRUSS, DSA100) to determine the membrane hydrophilicity. The concentration for organic contaminant in the simulated pollution water before and after desalination was detected by FTIR spectra instrument (VERTEX 80 V, Bruker). The solar absorption spectra were obtained using a UV–vis spectrometer (Lambda 950, PerkinElmer) equipped with an integrating sphere. The solar absorptivity (σ) was calculated by deducting transmittance (T = 0) and reflectance (R) from the incident light as following.

$$\sigma = 1 - R = \frac{\int_{300}^{2500} I(1-R)\mathrm{d}\lambda}{\int_{300}^{2500} I\mathrm{d}\lambda}$$

In which λ is wavelength, $I(\lambda)$ is the light intensity at different wavelengths.

Solar evaporation measurements

The solar evaporation performance was evaluated under 1 kW m^{-2} (CEL-PE300L Xenon lamp). We used an optical power meter to measure the illumination intensity. The synthetic hydrogels were fixed on the liquid surface for the solar evaporation test. The mass change of the residual liquid was recorded using an electronic analytical balance. An infrared camera (E8, FLIR, US) was used to measure the surface and infrared photographs.

Results and discussion

The synthesis procedure of $FeCoNiCrO_x$ through sol–gel method and high temperature calcination is illustrated in Fig. 1. First, metal nitrate precursors were mixed and crosslinked to homogeneously disperse metal cations in a gel mixture. During this process, Co^{2+} was oxidized to Co^{3+}, simultaneously ensuring the dispersion of Ni, Fe and Cr species. Afterwards, the mixture was calcined in Ar/N_2 to gain the FCNCO powders. By combining the oxides with highly absorbent hydrogel at different mass ratios, we synthesized a series of solar evaporators. The details of the synthetic method can be found in Experimental Section. Considering that the excellent light harvesting capacity and ultrafast water transport through the hierarchically pillar hydrogel matrix, the FCNCO-based hydrogel can be potentially applied as a high-efficiency solar evaporator benefited from effective photothermal conversion.

To confirm the formation of the phase of the FCNCO, we have conducted X-ray diffraction (XRD) measurement. The XRD pattern in Fig. 2a showed that the characteristic peaks of spinel oxides at 2θ = 18°, 30°, 36°, 37°, 43°, 53°, 57°53°, 57° and 63° [26]. Rietveld refinement of experimental XRD pattern was employed to determine the phase structure of the FCNCO. The initial structural model was built based on the spinel-structured Fd-3 m $A^{II}B_2^{III}O_4$ (A, B = Fe, Co, Ni, Cr). According to the results of Rietveld analysis, the lowest weighted profiles R-factor

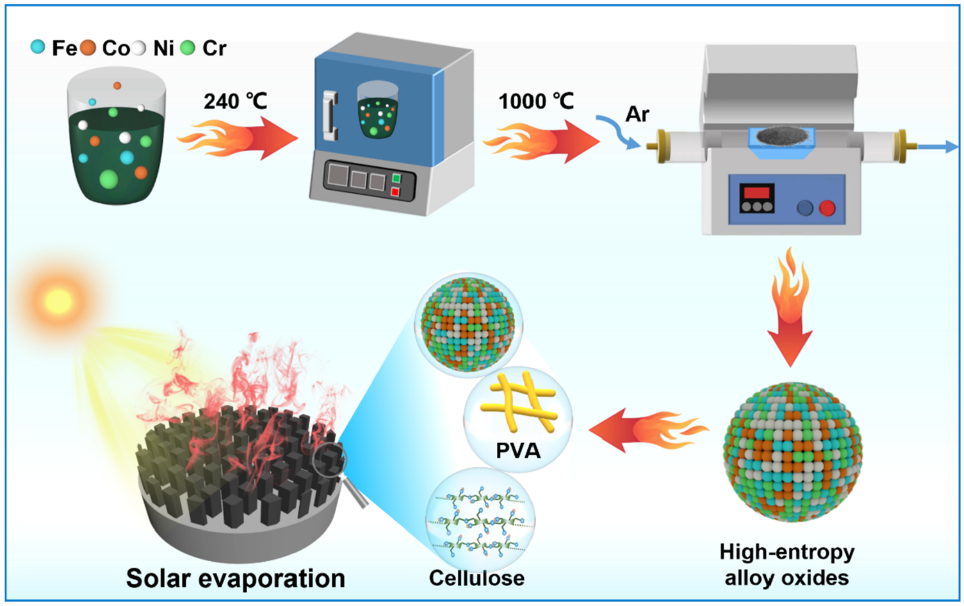

Figure 1 Schematic representation of the preparation process and application of hierarchically pillar hydrogel solar evaporator made of mixed metal oxides.

(w*R*p (%) = 6.8) and *R*-factor (*R*p (%) = 3.7) for the fitting model using $CoCr_2O_4$ demonstrated that Fe and Ni cations occupied the ternary metal $CoCr_2O_4$ due to chemical cation exchange and thermal oxidation process. Therefore, the synthesized mixed oxide was named as Fe-Co–Ni-Cr-O_x (FCNCO) according to the amounts of precursor metal ions. To further analyze the morphologies of the as-synthesized FCNCO, scanning electron microscopy was performed (Fig. 2b–d). We observed the obvious nanoparticles agglomeration, in which the $FeCoNiCrO_x$ consists of irregular particles with the sizes ranging from tens of nanometers to hundreds of nanometers. From Fig. 2e and f, the broaden vibration band at around 600 cm^{-1} belongs to the asymmetric metal–oxygen stretching vibrations, verifying the existence of different multi-transition metals. In the spectrum of the hydrogel, the peaks at 1075 cm^{-1}, 1375 cm^{-1} and 1721 cm^{-1} are attributed to the –C–OH, –CH_3 and C–C–O stretching vibrations.

The CPHs were prepared using these synthesized powders and further modified by pillar arrays to enhance the solar evaporation performance. Figure 3 shows the microstructure of the synthesized CPH-0 and CPH-2. All the hydrogels feature micro-sized porous structures with interconnected channels and thin walls. These macroporous capillary channels is beneficial for internal water transport. Higher magnification images revealed that the particles indeed penetrate the porous networks with the sizes ranging from hundreds of nanometers to several micrometers. In addition, we can easily observe the macroscopic feature of the CPHs-2 from the photograph (Fig. 4a). The pillar arrays can harvest light from all the directions and enlarge the evaporation areas, which can enhance photothermal conversion and evaporation efficiency. Moreover, light incident on transition metallic oxides can generate plasmonic resonance waveguides, which will redshift to the long-wavelength range (Fig. 4b). The 3d electrons at Fermi level of transition-metal ions can reduce plasma frequencies, leading to strong absorption over the UV–vis-IR spectrum. Moreover, this surface plasmon resonance could further decays to photoinduced hot electron via Landau damping and aggravate the Joule effect driven heat generation. Furthermore, the full solar spectrum absorption and efficient photothermal conversion achieved by plasmonic resonance effect will lead to a high-water evaporation rate [27]. Apart from the structural characteristics, the hydrophilicity and photothermal conversion capacities are critical for solar water evaporation. To intuitively investigate the water absorbing capability of the evaporator surface, we have conducted water contact angle measurement. A contact angle camera was employed to observe the impregnation process of water drops to affirm the surface wettability (Fig. 4c). It is seen that the impregnation process of the CPHs entirely finished within 1 s, which implying that the CPHs can be supplied with a continuous water flow quickly. Therefore, the as-prepared CPHs possessed

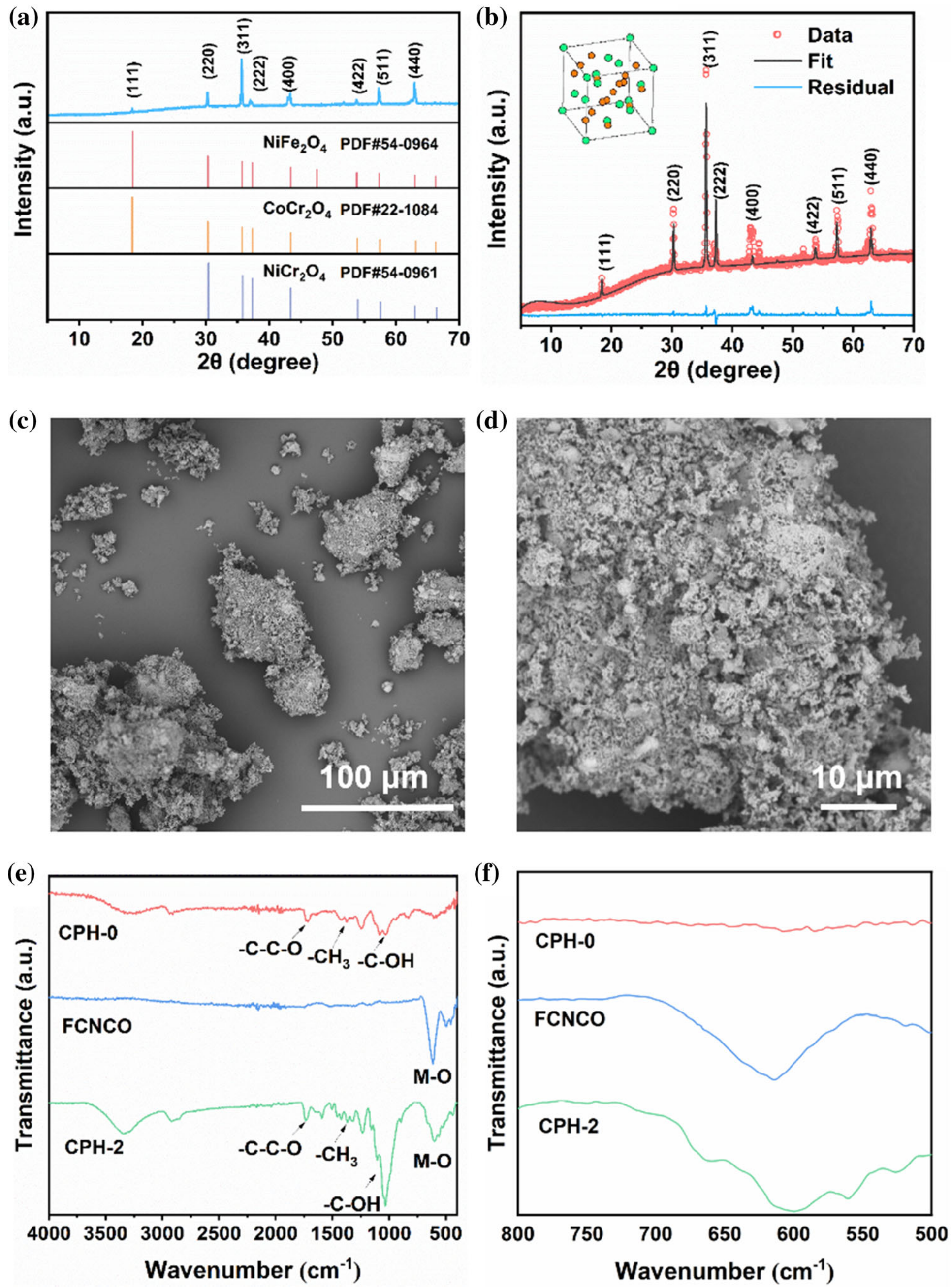

Figure 2 **a** XRD patterns, **b** The corresponding Rietveld refinement for FCNCO, **c**, **d** SEM images of FCNCO powder, **e**, **f** FTIR spectra of CPH-0, FCNCO and CPH-2.

hydrophilic surfaces to be wetted easily due to the inherent superior wicking and capillary effect of hydrogels, which were favorable for pumping water for evaporation.

We next examined the light absorption of the CPHs across the UV–Vis-NIR regions, which are shown in Fig. 4a. In our previous work, surface topography was demonstrated to enhance light absorption and accelerate water flow rate near the surface [24, 25]. Therefore, we constructed pillar arrays on the hydrogel surface to trap solar light and promote thermal conversion. For the hydrogels without surface structures, the light absorption was around 80% in the UV–Vis range. Whereas the CPH-2S exhibited the light absorption of 92% over the UV–Vis-NIR region, indicating that the solar absorptivity was significantly dominated by the surface structure of the hydrogels. Upon light irradiation, the absorbed light could quickly be converted into heat. The surface temperature of the CPH-2S (wet state) reached an equilibrium temperature of 43 °C (Fig. 4b), which is beneficial for solar evaporation. To explore the

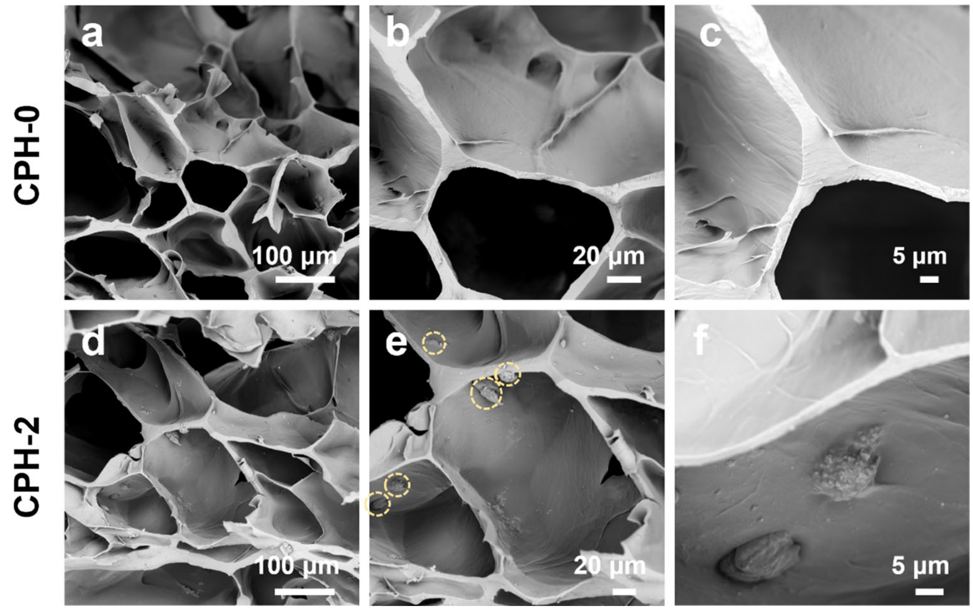

Figure 3 **a**–**c** SEM images of CPH-0 hydrogel, **b**–**d** SEM images of CPH-2 hydrogel.

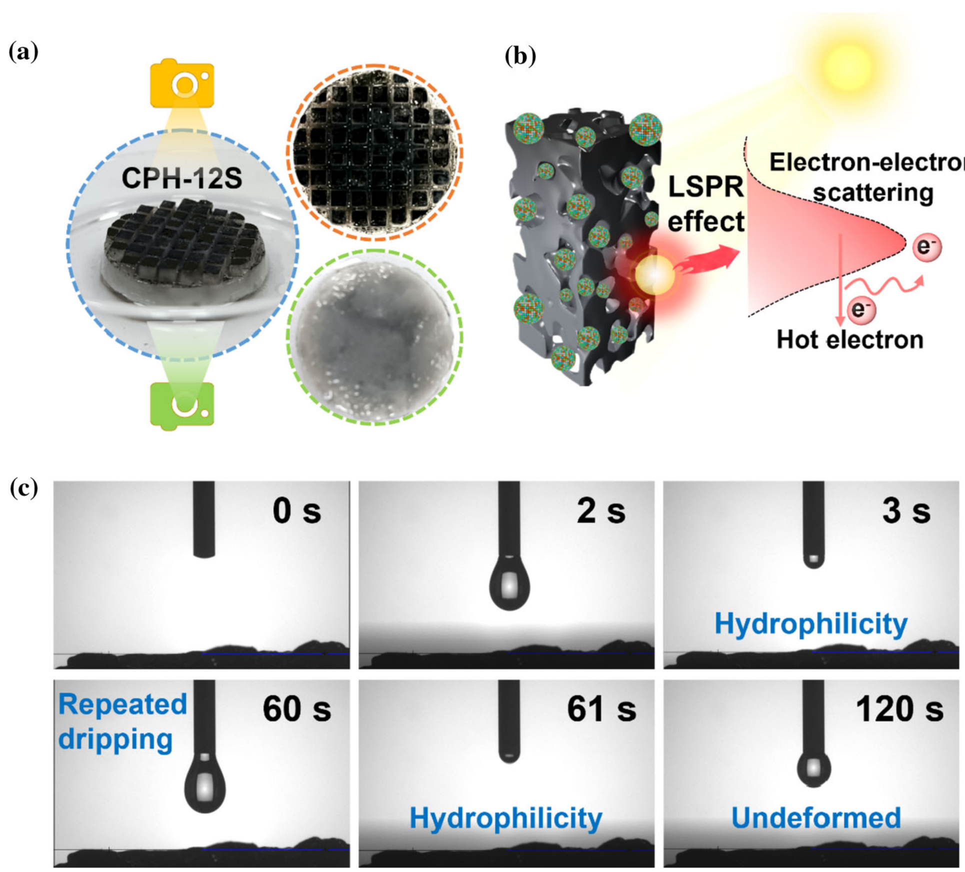

Figure 4 **a** Schematic illustration of the structure of solar evaporator, **b** Schematic illustration of the general mechanism for light trapping and photothermal conversion, **c** The time-lapse snapshots of absorption of a water droplet by the CPH-2.

solar evaporation ability, the CPHs were floated on water and seawater, respectively. Figure 5 exhibited that the mass of the liquid decreased with the increasing irradiation time. The average water evaporation rates of CPH-2 reached 2.22 kg·m^{-2}·h^{-1}, which was 6, 2.92 and 1.11 times higher than the evaporation of pure water, CPH-0 and CPH-1. Notably, as the surface of the CPH-2 was molded into that of CPH-2S, the evaporation rate dramatically increased from 2.22 to 2.44 kg·m^{-2}·h^{-1}, deriving from

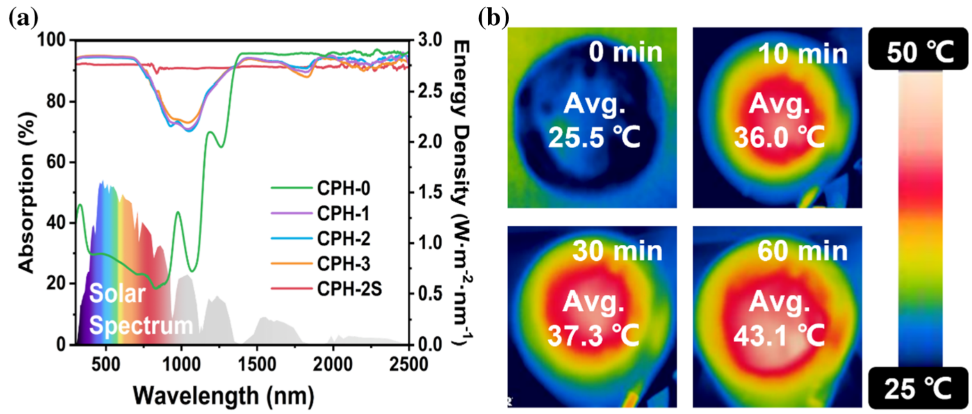

Figure 5 **a** Solar absorptivity of CPH-0, CPH-1, CPH-2, CPH-3 and CPH-2S; **b** The temperature distribution of the CPH-2S captured by E8 infrared camera.

the additional evaporation by the side area of the pillar arrays. These results indicated that the synergistic of light trapping effect and side area-assisted evaporation is conducive to promote solar evaporation.

In addition, the light to vapor efficiency (η) of the evaporator is determined by the percentage of the energy for water evaporation in comparison to the total energy of the incident light, that is the following equation [28]:

$$\eta = \frac{v \cdot H_{LV}}{P_{Sun}}$$

in which v is solar evaporation rate, H_{LV} is the energy for the phase change from liquid to gas of water, P_{sun} is the intensity of incident light. The corresponding solar evaporation efficiency for CPH-0, CPH-1, CPH-2, CPH-3 and CPH-2S was 32%, 79%, 87%, 87%, and 96%. Such high efficiency was caused by the synergy of excellent photothermal conversion and low evaporation enthalpy of water. Besides, excellent anti-salt accumulation property of the CPHs is crucial for durable solar desalination performance. The solar evaporation performance for the CPHs in seawater was also investigated, in which the CPHs evaporated sodium chloride solution (NaCl) of different salinities to explore the solar desalination capability. It was found that the average evaporation rates for CPH-2S in all the seawater was nearly same as that in water (Fig. 5c and d). Under continuous solar irradiation, the solar evaporation rate did not change obviously, indicating a stable solar desalination performance (Fig. 6a). Meanwhile, the CPH-2S exhibited one of the highest efficiencies compared with other reported evaporators (Fig. 6b) [28–33]. We also constructed the spectral absorptivity of organic sewages (MB, MO) and condensed water to assess the solar purification performance. As shown in Fig. 6c, the collected water became colorless, as well as the absorption peak of MB and MO, vanished after solar evaporation.

Conclusion

In summary, an efficient solar evaporator was prepared by combining mixed metal oxides $FeCoNiCrO_x$ with a polymer-based hydrogel, which can significantly purified seawater or organic sewage powder by solar energy. Coupled with the pillar arrays design of surface topography, the 3D pillar hydrogel solar evaporator enabled a rate of 2.44 kg m^{-2} h^{-1} under one sun irradiation, about 700% of the nature water evaporation rate. The corresponding energy efficiency was up to 96% (Fig. 7). Even during a long-term solar desalination, the evaporator maintained desired anti-salt accumulation capacity and a stable solar evaporation performance. The energy-saving solar thermal conversion capacity endows the 3D pillar hydrogel with the potential applications in a facile, efficient and stable solar desalination.

Acknowledgements

This work was supported by the National Natural Science Foundation of China (51902164). This work was also funded by the Priority Academic Program Development of Jiangsu Higher Education Institutions (PAPD).

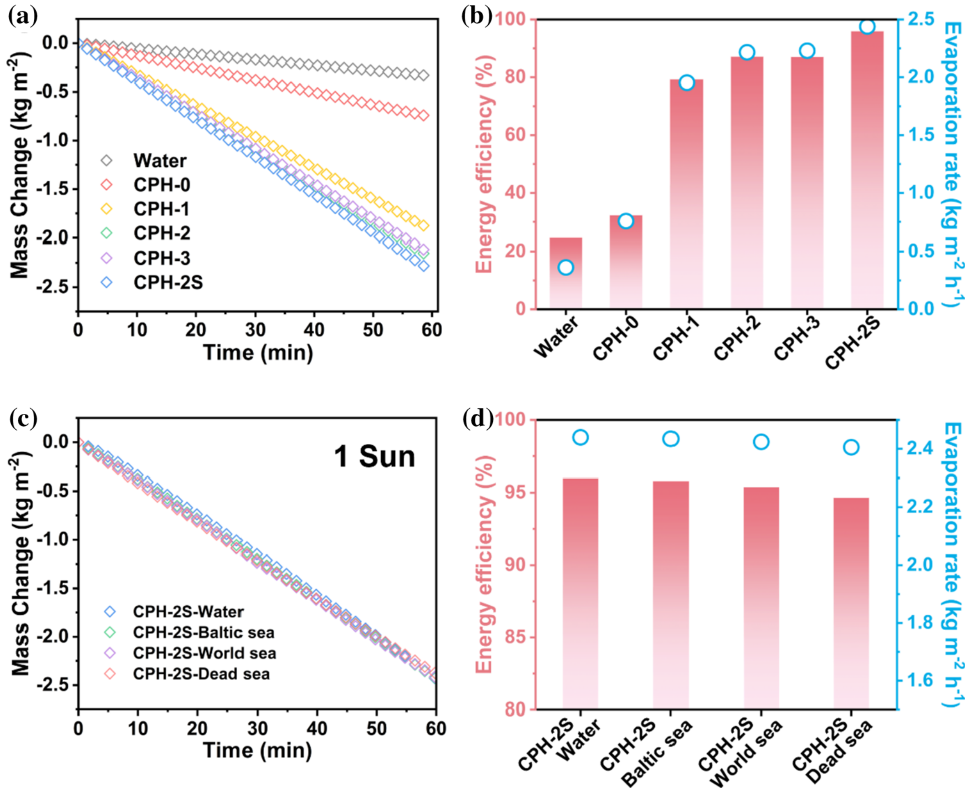

Figure 6 **a** Mass change, **b** (red bar) light to vapor efficiency, (blue circle) evaporation rate of different evaporators and water during solar water evaporation, and **c** mass change, **d** (red bar) light to vapor efficiency, (blue circle) evaporation rate of different evaporators during solar desalination.

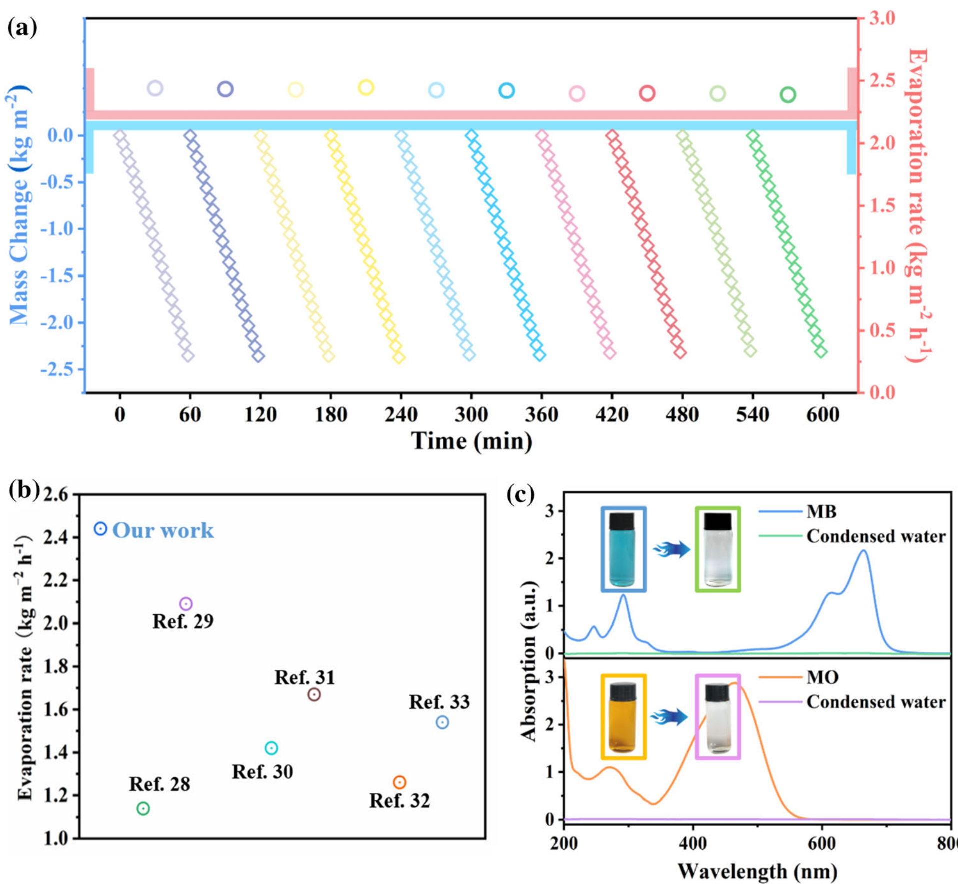

Figure 7 **a** The cyclic performance of solar evaporation for the CPH-2S at one sun illumination, **b** The evaporation rate of the CPH-2S in comparison with those metallic oxides-based materials employ as solar evaporators, **c** The absorbency of MB or MO solutions and evaporated water.

Author contributions

HM: Performed the experiment and drafted the manuscript. DF and HZ prepared the materials and performed the experiments. XX assisted the data analysis and discussion. XY and YL supervised the project and finalized the manuscript. All authors have given approval to the final manuscript.

Declarations

Conflicts of interest The authors declare no conflict of interest that could have appeared to influence the work reported in this paper.

References

[1] Wang YY, Zhang JN, Balogun M-S, Tong YX, Huang YC (2022) Oxygen vacancyebased metal oxides photoanodes in photoelectrochemical water splitting. Mater Today Sustain 18:100118. https://doi.org/10.1016/j.mtsust.2022.100118

[2] Ding T, Ho GW (2021) Using the sun to co-generate electricity and freshwater. Joule 5:1639–1641. https://doi.org/10.1016/j.joule.2021.06.021

[3] Cui SS, Liu X, Shi YB, Ding MY, Yang XF (2022) Construction of atomic-level charge transfer channel in $Bi_{12}O_{17}Cl_2$/MXene heterojunctions for improved visible-light photocatalytic performance. Rare Met 41:2405–2416. https://doi.org/10.1007/s12598-022-02011-3

[4] Ding C, Zhao CX, Cheng S, Yang XF (2022) Ultrahigh photocatalytic hydrogen evolution performance of coupled 1D CdS/1T-phase dominated 2D WS_2 nanoheterojunctions. Chin J Catal 43:403–409. https://doi.org/10.1016/S1872-2067(21)63844-5

[5] Huang YC, Xu HM, Yang HJ, Lin Y, Liu H, Tong YX (2018) Efficient charges separation using advanced BiOI-based hollow spheres decorated with palladium and manganese dioxide nanoparticles. ACS Sustain Chem Eng 6:2751–2757. https://doi.org/10.1021/acssuschemeng.7b04435

[6] Pang Y, Zhang J, Ma R, Qu Z, Lee E, Luo T (2020) Solar–thermal water evaporation: a review. ACS Energy Lett 5:437–456. https://doi.org/10.1021/acsenergylett.9b02611

[7] Wang Y, Wu X, Gao T, Lu Y, Yang X, Chen GY, Owens G, Xu H (2021) Same materials, bigger output: a reversibly transformable 2D–3D photothermal evaporator for highly efficient solar steam generation. Nano Energy 79:105477. https://doi.org/10.1016/j.nanoen.2020.105477

[8] Shen Z, Fan D, Zhang H, Jing J, Xu H, Min H, Lu Y, Yang X, Xu J (2022) Integrating a metal–organic framework into natural spruce wood for efficient solar-powered water evaporation. Sol RRL. https://doi.org/10.1002/solr.202200483

[9] Lu Y, Zhang H, Fan D, Chen Z, Yang X (2022) Coupling solar-driven photothermal effect into photocatalysis for sustainable water treatment. J Hazard Mater 423:127128. https://doi.org/10.1016/j.jhazmat.2021.127128

[10] Xu Y, Xu J, Zhang J, Li X, Fu B, Song C, Shang W, Tao P, Deng T (2022) All-in-one polymer sponge composite 3D evaporators for simultaneous high-flux solar-thermal desalination and electricity generation. Nano Energy 93:106882. https://doi.org/10.1016/j.nanoen.2021.106882

[11] Meng S, Tang CY, Jia J, Yang J, Yang MB, Yang W (2022) A wave-driven piezoelectric solar evaporator for water purification. Adv Energy Mater 12:2200087. https://doi.org/10.1002/aenm.202200087

[12] Wu X, Wu Z, Wang Y, Gao T, Li Q, Xu H (2021) All-cold evaporation under one sun with zero energy loss by using a heatsink inspired solar evaporator. Adv Sci 8:2002501. https://doi.org/10.1002/advs.202002501

[13] Wu X, Wang Y, Wu P, Zhao J, Lu Y, Yang X, Xu H (2021) Dual-zone photothermal evaporator for antisalt accumulation and highly efficient solar steam generation. Adv Funct Mater 31:2102618. https://doi.org/10.1002/adfm.202102618

[14] Huang YC, Lu YR, Lin Y, Mao YC, Ouyang GF, Liu H, Zhang SQ, Tong YX (2018) Cerium-based hybrid nanorods for synergetic photo-thermocatalytic degradation of organic pollutants. J Mater Chem A 6:24740. https://doi.org/10.1039/c8ta06565a

[15] Fan D, Min H, Zhang H, Tang Y, Yang X, Lu Y (2021) Architecting a bifunctional solar evaporator of perovskite $La_{0.5}Sr_{0.5}CoO_3$ for solar evaporation and degradation. J Mater Sci 56:18625–18635. https://doi.org/10.1007/s10853-021-06420-0

[16] Zhao J, Bao J, Yang S, Niu Q, Xie R, Zhang Q, Chen M, Zhang P, Dai S (2021) Exsolution–dissolution of supported metals on high-entropy $Co_3MnNiCuZnO_x$: Toward sintering-resistant catalysis. ACS Catal 11:12247–12257. https://doi.org/10.1021/acscatal.1c03228

[17] Ye KH, Hu P, Liu KL, Tang ST, Huang D, Lin Z, Zhang SQ, Huang YC, Ji HB, Yang SH (2022) New findings for the much-promised hematite photoanodes with gradient doping and overlayer elaboration. Sol RRL. https://doi.org/10.1002/solr.202100701

[18] Yang W, Hou LQ, Wang P, Li Y, Li R, Jiang B, Yang F, Li YF (2022) High mass loading $NiCo_2O_4$ with shell-nanosheet/core-nanocage hierarchical structure for high-rate solid-state hybrid supercapacitors. Green Energy Environ 4:723–733. https://doi.org/10.1016/j.gee.2020.11.014

[19] Li Y, Liao Y, Zhang J, Huang E, Ji L, Zhang Z, Zhao R, Zhang Z, Yang B, Zhang Y, Xu B, Qin G, Zhang X (2021) High-entropy-alloy nanoparticles with enhanced interband transitions for efficient photothermal conversion. Angew Chem Int Ed 60:27113–27118. https://doi.org/10.1002/anie.202112520

[20] He CY, Gao XH, Qiu XL, Yu DM, Guo HX, Liu G (2021) Scalable and ultrathin high-temperature solar selective absorbing coatings based on the high-entropy nanoceramic AlCrWTaNbTiN with high photothermal conversion efficiency. Sol RRL 5:2000790. https://doi.org/10.1002/solr.202000790

[21] Divya VK, Abraham KE (2019) Multifunctional transition metal doped Sb_2O_3 thin film with high near-IR transmittance, anti-reflectance and UV blocking features. Appl Surf Sci 493:1115–1124. https://doi.org/10.1016/j.apsusc.2019.07.062

[22] Ming X, Guo A, Wang G, Wang X (2018) Two-dimensional defective tungsten oxide nanosheets as high performance photo-absorbers for efficient solar steam generation. Sol Energ Mater Sol C 185:333–341. https://doi.org/10.1016/j.solmat.2018.05.049

[23] Lu Q, Yang Y, Feng J, Wang X (2019) Oxygen-defected molybdenum oxides hierarchical nanostructure constructed by atomic-level thickness nanosheets as an efficient absorber for solar steam generation. Sol RRL 3:1800277. https://doi.org/10.1002/solr.201800277

[24] Fan D, Lu Y, Zhang H, Xu H, Lu C, Tang Y, Yang X (2021) Synergy of photocatalysis and photothermal effect in integrated 0D perovskite oxide/2D MXene heterostructures for simultaneous water purification and solar steam generation. Appl Catal B: Environ 295:120285. https://doi.org/10.1016/j.apcatb.2021.120285

[25] Lu Y, Fan D, Wang Y, Xu H, Lu C, Yang X (2021) Surface patterning of two-dimensional nanostructure-embedded photothermal hydrogels for high-yield solar steam generation. ACS Nano 15:10366–10376. https://doi.org/10.1021/acsnano.1c02578

[26] Sun Y, Ren X, Sun S, Liu Z, Xi S, Xu ZJ (2021) Engineering high-spinstate cobalt cations in spinel zinc cobalt oxide for spin channel propagation and active site enhancement in water oxidation. Angew Chem Int Ed 60:14536–14544. https://doi.org/10.1002/anie.202102452

[27] Ibrahim I, Seo DH, McDonagh AM, Shon HK, Tijing L (2021) Semiconductor photothermal materials enabling efficient solar steam generation toward desalination and wastewater treatment. Desalination 500:114853. https://doi.org/10.1016/j.desal.2020.114853

[28] Li W, Li X, Liu J, Zeng MJ, Feng X, Jia X, Yu ZZ (2021) Coating of wood with Fe_2O_3-decorated carbon nanotubes by one-step combustion for efficient solar steam generation. ACS Appl Mater Interfaces 13:22845–22854. https://doi.org/10.1021/acsami.1c03388

[29] Zuo S, Xia D, Guan Z, Yang F, Cheng S, Xu H, Wan R, Li D, Liu M (2021) Dual-functional CuO/CN for highly efficient solar evaporation and water purification. Sep Purif Technol 254:117611. https://doi.org/10.1016/j.seppur.2020.117611

[30] Wang W, Yan X, Geng J, Zhao N, Liu L, Vogel T, Guo Q, Ge L, Luo B, Zhao Y (2021) Engineering a copper@polypyrrole nanowire network in the near field for plasmon-enhanced solar evaporation. ACS Nano 15:16376–16394. https://doi.org/10.1021/acsnano.1c05789

[31] Wang Y, Wang C, Liang W, Song X, Zhang Y, Huang M, Jiang H (2020) Multifunctional perovskite oxide for efficient solar-driven evaporation and energy-saving regeneration. Nano Energy 70:104538. https://doi.org/10.1016/j.nanoen.2020.104538

[32] Dong YY, Cao LT, Si Y, Ding B, Deng HB (2020) Cellular structured CNTs@SiO nanofibrous aerogels with vertically aligned vessels for salt-resistant solar desalination. Adv Mater 32:1908269. https://doi.org/10.1002/adma.201908269

[33] Zhang J, Yang Y, Zhao J, Dai Z, Liu W, Chen C, Gao S, Golosov DA, Zavadski SM, Melnikov SN (2019) Shape tailored Cu_2ZnSnS_4 nanosheet aggregates for high efficiency solar desalination. Mater Res Bull 118:110529. https://doi.org/10.1016/j.materresbull.2019.110529